Nano World Journal

https://doi.org/10.17756/nwj.2023-s2-047

Research Article

Open Access

Chloride Permeability of Aerated Alkali-activated Mortar Based on Electric Arc Furnace Slag and Fly Ash

Fatima Ouzoun*, Azzedine Moussadik, Hind Agourrame, Hassan Ez-zaki, Mohamed Saadi and Abdeljebbar Diouri

Laboratory of Applied Materials Chemistry, Faculty of Sciences, Mohammed V University in Rabat, Morocco

***Correspondence to:**
Fatima Ouzoun
Laboratory of Applied Materials Chemistry,
Faculty of Sciences,
Mohammed V University in Rabat, Morocco.
E-mail: fatima.ouzoun@um5r.ac.ma

Received: July 25, 2023
Accepted: September 26, 2023
Published: September 27, 2023

Citation: Ouzoun F, Moussadik A, Agourrame H, Ez-zaki H, Saadi M, et al. 2023. Chloride Permeability of Aerated Alkali-activated Mortar Based on Electric Arc Furnace Slag and Fly Ash. *NanoWorld J* 9(S2): S274-S280.

Copyright: © 2023 Ouzoun et al. This is an Open Access article distributed under the terms of the Creative Commons Attribution 4.0 International License (CCBY) (http://creativecommons.org/licenses/by/4.0/) which permits commercial use, including reproduction, adaptation, and distribution of the article provided the original author and source are credited.

Published by United Scientific Group

Abstract

The objective of this study is to develop aerated alkali-activated mortar based on electric arc furnace slag (EAFS) and class F fly ash (FA) and investigate the effect of these different by-products on the resistance of the mortar to chloride penetration. Three variations of lightweight alkali-activated binder mortars were prepared by partially substituting cement and sand with Moroccan local by-products, namely EAFS and class F FA. A 4 M sodium hydroxide (NaOH) solution was used as an alkali activator in the mixture. The mortar specimens were cured in water at 20 ± 2 °C for 28 days at room temperature, followed by exposure to a chloride solution (0.5 M of NaCl) for 10 and 30 days. Characterization of the mortars was carried out using the X-ray fluorescence (XRF) technique to determine the elemental composition and X-ray diffraction (XRD) to identify the phases present. The XRD results obtained after 28 days of curing indicated the presence of hydrated calcium aluminate silicate (C-A-S-H) and hydrated alkaline aluminate (N-A-S-H) phases in the mortars. The formation of these phases impacts mortar's resistance to chloride ingress. The results obtained after 10 and 30 days of exposure to saline solution, revealing that a higher content of EAFS, which promotes the formation of the C-A-S-H gel, significantly enhances the mortar's resistance to chloride penetration.

Keywords

Chloride diffusion resistance, Aerated concrete, Electric arc furnace slag, Fly ash

Introduction

The production of ordinary Portland cement (OPC) has been associated with the release of significant amounts of CO_2 into the atmosphere which exacerbates global warming [1]. Therefore, the research focused on producing alkali-activated materials as alternative binders. Through alkali activation, industry waste can be reused efficiently. Mortar and concrete with alkali-activated ground granulated blast furnace slag (GGBS), FA, and silica fume blended binders in combination with OPC in optimum quantities is known to enhance most concrete properties of interest to the construction industry [2]. Two types of binding systems can be classified based on the chemical composition of the raw materials: one is the alkali activated slag (Si + Ca) system, having a C-A-S-H type gel with a low Ca/Si ratio and a high Al incorporation as the main reaction product, giving rise to a structure similar to that of the minerals known as tobermorite [3-5]. The other is the alkali activated class F FA/metakaolin (Si + Al) system, having N-A-S-H type gels which is less dense with a more permeable pore system than C-A-S-H [4]. Precursors rich in calcium are more reactive when placed in solutions of moderate alkalinity compared to precursors with low calcium content. Consequently, the range of activators for the slag will be much broader, as in addition to

hydroxides and silicates, sulphates and alkali metal carbonates are used. The combination of FA and slag in alkali-activated binders impart additional favorable properties as they tend to compensate for the shortcomings of each other [6]. Alkali-activated cement is widely applicable in various members of construction, and aerated concrete is one of them.

Aerated concrete is a type of porous lightweight building material widely used in wall insulation [7]. It is developed to improve some characteristics, such as weight reduction, water permeability, and thermal insulation. Its properties have been enhanced with many mineral admixtures, calcium-containing materials (cement and lime), silica-containing materials (sand, FA, etc.), and materials used for foaming [foaming agent [8, 9], metallic powder (Al, Zn) [10-12] or hydrogen peroxide (H_2O_2) [13]. The most commonly used material for foaming is Al powder as mentioned in several previous studies [11, 13, 14]. It has been reported that the H_2 gas generated by the reaction of Zn powder (Equation 1) is about half in quantity compared with Al powder and causes a relatively slow foaming reaction [15]. Studies on OPC-based [16] and FA-based geopolymer [17] or magnesium phosphate [10] have been reported for expanded cement/concrete using Zn powder, however, studies on alkali activated slag are still insufficient.

$$Zn + 2OH^- + 2H_2O \rightarrow \left[Zn(OH)_4\right]^{2-} + H_2 \uparrow \quad (1)$$

The eminent financial and environmental impact of restoring and replacing damaged structures and elements after a few years of service is increasingly taken seriously [18]. The factor impacting the degradation of reinforced concrete is the reaction of aggressive agents, and their diffusivity within the cementitious matrix [4]. The most valued aspect of concrete durability is the attack of chlorides. They may penetrate by capillary absorption, hydrostatic pressure, and/or diffusion of ions. Thus, even though concrete matrix is not significantly harmed by the chlorides but they promote the corrosion of the embedded steel bars leading to its structural collapse [19]. Several studies have reported that alkali-activated materials exhibited a more compact pore structure and thus higher chloride resistance than Portland cement-based materials [20]. The authors [20, 21] attributed this relatively high durability mainly to the lower Ca/Si ratio of the binder matrix because of the absence of Portlandite ($Ca(OH)_2$) in the composition of this type of materials and extremely low permeability.

Therefore, this study has two purposes. The first is the development of aerated alkali-activated binder mortar by using two by-products (EAFS and FA) and Zn powder as the foaming agent. The second is to evaluate their impact on resistance against chloride diffusion of mortar.

Materials and Method

Materials

The used materials for this study include natural sand consists of crystalline silica, EAFS comes from the SONASID-Jorf steel plant in Morocco, FA from the Safi thermal power plant, and OPC (type CPJ35). The solid mixture was mixed with NaOH (4 M). The materials used are nanoscale.

Mortar preparation

Three specimens were prepared and tested in this study. The mixtures were designed to partially substitute FA and lime with EAFS. Zinc powder was used as the foaming agent, and alkali activation was carried out by hydrating the mixtures with NaOH solution (4 M). To prepare the specimens, the solid-state mixture was first ground in a laboratory mill which involved mechanical activation to enhance the reactivity of the precursors. Then, the NaOH solution was gradually added while continuously mixing the ingredients to ensure uniform distribution. This step aimed to achieve proper activation and chemical reaction within the mortar. Following the mixing process, the mortars were cast into cylindrical molds with a diameter of 4.5 cm. After two days of ambient drying, the molded mortar specimens were demolded and subsequently cured in water at a temperature of 20 ± 2 °C for a total duration of 28 days. This curing condition was selected to provide a moist environment that supports the hydration process and strength development of the mortar samples. Table 1 provides a comprehensive summary of the mortar mixtures studied, including their corresponding mix proportions.

Table 1: Mortar mix proportions (% mass).

Mix	EAFS	FA	Lime	Sand	CPJ35	Gypsum	Zn
M1	25	10	7	50	5	1	2
M2	30	7	5	50	5	1	2
M3	35	5	2	50	5	1	2

Chloride diffusion test

The test procedure is described as mentioned in the LCPC test method No. 58 [22]. After 28 days of curing, the samples were immersed in a NaOH solution (0.1 M) under a vacuum for 24 h; the choice of saturation with a strongly basic solution comes from the fact that it maximizes the penetration of free chlorides into the cement matrix [23]. Surfaces of mortars were sealed with a polyurethane resin and only the bottom surface was exposed to the saline solution NaCl (0.5 M) to ensure one-dimensional diffusion. The solution level was maintained at 10 mm above the bottom surface of the specimen, and the solution was renewed every 5 days. After 10 and 30 days, specimens were taken out from the NaCl solution and split into two identical halves; the first one was used to determine chloride penetration depth by spraying a silver nitrate solution (0.1 M), which was measured from white silver chloride precipitation. The apparent chloride diffusion coefficient was calculated from the measured X_d using equation 2. The second half of each specimen was cut into three 5 mm thick slices. Each slice was ground into fine powder to measure the chloride content according to the chemical titration [24].

$$D_{app} = \frac{X^2}{4t} \quad (2)$$

Where $\mathbf{D}_{app}$ is the apparent chloride diffusion coefficient (m^2/s), X is chloride penetration depth (m), and **t** is the exposure time (s).

Results and Discussion

X-ray fluorescence

The XRF analysis of EAFS and FA is presented in table 2. EAFS is rich in oxide calcium and iron oxide since this slag is extracted during the first melting process. According to the literature, slag with $CaO/(SiO_2 + P_2O_5) > 1.8$ may contain some quantity of dicalcium silicate (C_2S) and tricalcium silicate (C_3S), it can be considered as cementitious material [25]. For EAFS used in this study $CaO/(SiO_2 + P_2O_5)$ ratio calculated from the chemical composition is equal to 2.43, which suggests that it may exhibit suitable cementitious hydraulic activity. FA has more than 80% of the mass percentage of SiO_2 and Al_2O_3 of the total weight, which means a rich source of aluminosilicates.

Table 2: Chemical composition of cement CPJ35, EAFS, and FA.

Oxides	EAFS	FA
CaO	26.05	1.711
Fe_2O_3	23.33	5.582
SiO_2	10.35	54.63
Al_2O_3	5.95	28.07
MgO	4.68	0.985
SO_3	0.27	0.3566
K_2O	0.05	2.338
TiO_2	0.48	1.711
Na_2O	-	0.3898
MnO	2.77	0.02178
P_2O_5	0.34	0.1672
BaO	-	0.1642
SrO	0.086	0.09227
LOI	24.80	3.7811

X-ray diffraction

The diffraction peaks of crystalline phases were identified using the Diamond 2.1d software from the CIF (Crystallographic Information File) files published in the literature [26]. The mineralogical composition of EAFS and FA samples, determined by the XRD method, is presented in figure 1 and figure 2, respectively. The X-ray diffractogram showed that the major mineralogical phases of EAFS were Larnite Ca_2SiO_4 (JCPDS card No.96-901-2791), Wuestite FeO (JCPDS card No.96-900-9768), Fayalite Fe_2SiO_4 (JCPDS card 71-1669), and Olivine $FeMgSiO_4$ (JCPDS card No.96-900-1670). The FA mainly consists of the crystallized phases: Quartz SiO_2 (JCPDS card No.96-210-6356), Mullite $3Al_2O_3$, $2SiO_2$ (JCPDS card No.15-776), and Wuestite FeO (JCPDS card No.96-900-8637).

X-ray diffractograms of the alkali-activated mortars after 28 days of curing are presented in figure 3. SiO_2 peaks are observed in the diffractograms, which is obvious since these mortars contain silica sand and unreacted FA, known for its high SiO_2 content. The presence of CaO in the matrix may have reacted with water leading to the formation of C-S-H (Nekoite: $Ca_3Si_6O_{15}.7H_2O$, JCPDS card No. 96-900-0790), as observed near 29.5° 2θ, it is one of the main products of alkali-activated slag as previously reported [25, 27]. Peaks corresponding to Zoisite $Ca_2Al_3Si_3O_{13}H$ (JCPDS card No. 96-901-4730), and

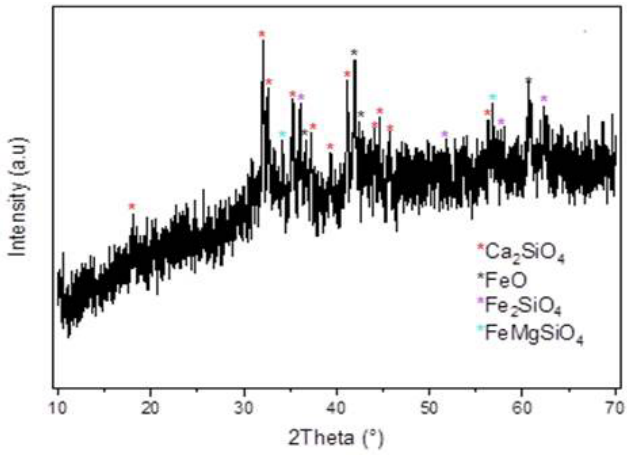

Figure 1: XRD of EAFS (Larnite: Ca_2SiO4, Wuestite: FeO, Fayalite: Fe_2SiO_4, and Olivine: $FeMgSiO_4$).

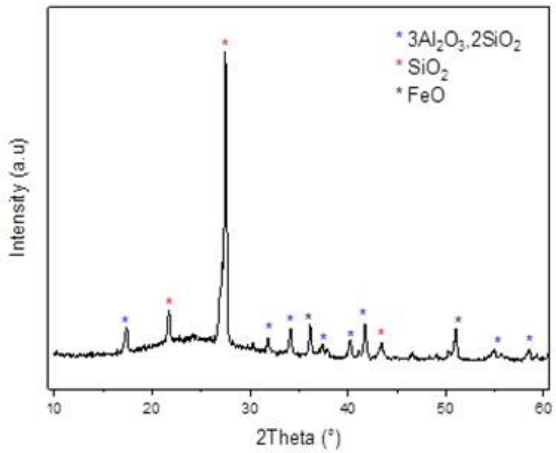

Figure 2: XRD of FA: (Mullite: $3Al_2O_3$, 2SiO2, Quartz: SiO_2, and Wuestite: FeO).

N-A-S-H gel (Analcime $NaAlSi_2O_6.H_2O$, JCPDS card No. 96-900-4014, a hydration product of FA) were observed in the first mixture (M1), which has the highest percentage of FA and the lowest percentage of slag. Moving from the 1st mix to the 3rd the percentage of FA is gradually replaced by slag, C-A-S-H gel (Gismondine $CaAl_2Si_2O_8.2H_2O$, JCPDS card No. 96-901-2417) peaks appeared, which is evident by increasing the amount of EAFS that contains a quantity of CaO that could improve the geopolymerization process and generate more gel, which is consistent with previous research [27]. Furthermore, the present of Calcite $CaCO_3$ (JCPDS card No. 96-901-6707) is detected, which may be attributed to slight carbonation during mixing, sample preparation, or measurements, as reported by other researchers [27, 28]. Some peaks of Wuestite (JCPDS card No. 96-900-8637) are also observed, indicating that this phase did not significantly participate in the activation reaction.

Water absorption

To understand the factors affecting the chloride diffusion in alkali activated fly ash slag (AAFS) mortars, water absorption of mortars with different FA/EAFS ration was measured as shown in figure 4. The water absorption content reflects the apparent pore volume in the AAFS. A significant percentage

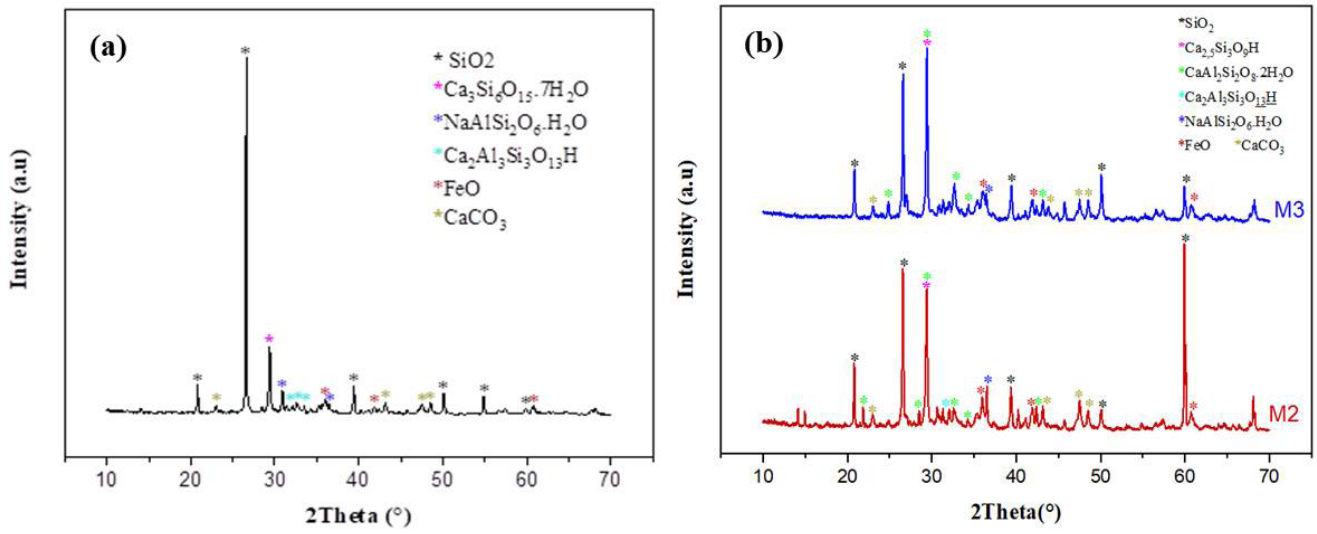

Figure 3: XRD of mortars **(a)** M1 and **(b)** M2 and M3: SiO_2: Quartz, $Ca_3Si_6O_{15}.7H_2O$: Nekoite, $Ca_2Al_3Si_3O_{13}H$: Zoisite, $CaAl_2Si_2O_8.2H_2O$: Gismondine, $NaAlSi_2O_6.H_2O$: Analcime, $CaCO_3$: Calcite, and FeO: Wuestite.

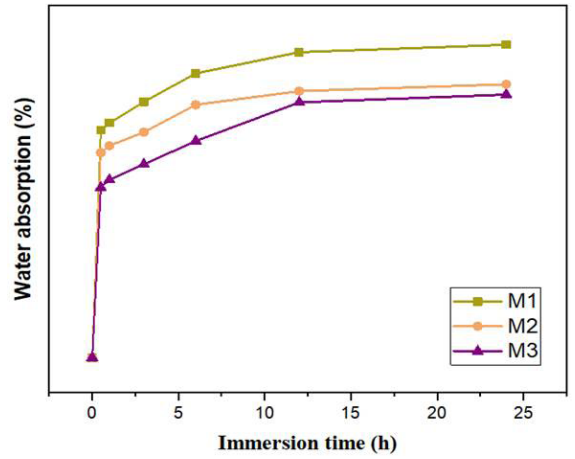

Figure 4: Water absorption of mortars M1-M3.

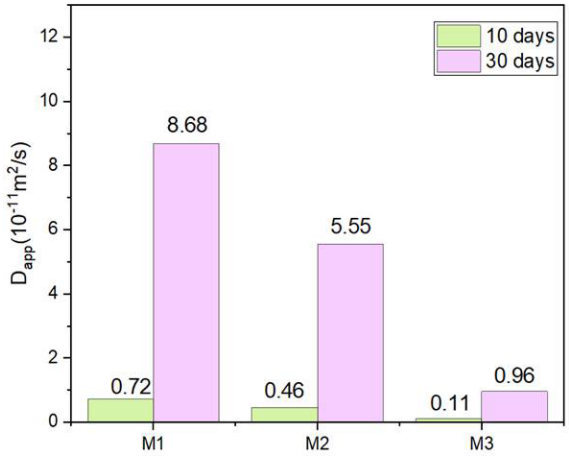

Figure 5: Apparent diffusion coefficients of EAFS/FA based mortars obtained at 10 and 30 days of saline exposure.

of water absorption was observed, which is evident from the fact that the samples are aerated by the Zn powder added to the mixture, which caused the samples to swell. The water absorption sharply increased and quickly got equilibrium. Mortars with lower slag content showed higher water absorption.

Chloride diffusion

Apparent diffusion coefficient

Chloride penetration depth was measured from the visible white silver chloride precipitation at two different exposure times to saline solution, 10 and 30 days. Chloride penetration depths and diffusion coefficients of FA/EAFS based mortars obtained at different exposure times to saline solution are in figure 5. It can be seen from figure 5 that after an exposure time of 10 and 30 days, FA replacement with EAFS reduced apparent chloride diffusion coefficient (D_{app}). While it is clearly shown that the effect of exposure time is as significant as that of the replacement level where D_{app} tended to increase after 30 days. Previous investigation indicated that in AAFS blended system, when the slag content was low, calcium ions tended to be adsorbed in N-A-S-H gels through charge balance. The formation of C-A-S-H gels, therefore, was limited. When the slag content > 50%, C-A-S-H gels were the major products formed in AAFS. Compared with N-A-S-H gels, C-A-S-H gels could incorporate water into their crystalline structure during hydration process [28]. As a result, pores were filled and the chloride resistance of AAFS concrete was improved. Therefore, in this study, for AAFS mortar with higher slag content, the D_{app} decreased. The result was consistent with the findings from previous researches [4, 28-31].

Chloride concentration profiles

Free and total chloride concentration profiles of FA and EAFS based mortars obtained after 10 and 30 days of exposure to saline solution are illustrated in figure 6. The free and total chloride content at exposure surface decreased along the depth, a higher content has been observed on the exposed external surface of all tested samples. As can be seen for all the alkali-activated samples, there is a remarkably good match between the total and free chloride profiles, revealing insignificant chemical chloride binding capacity [28]. While a lack

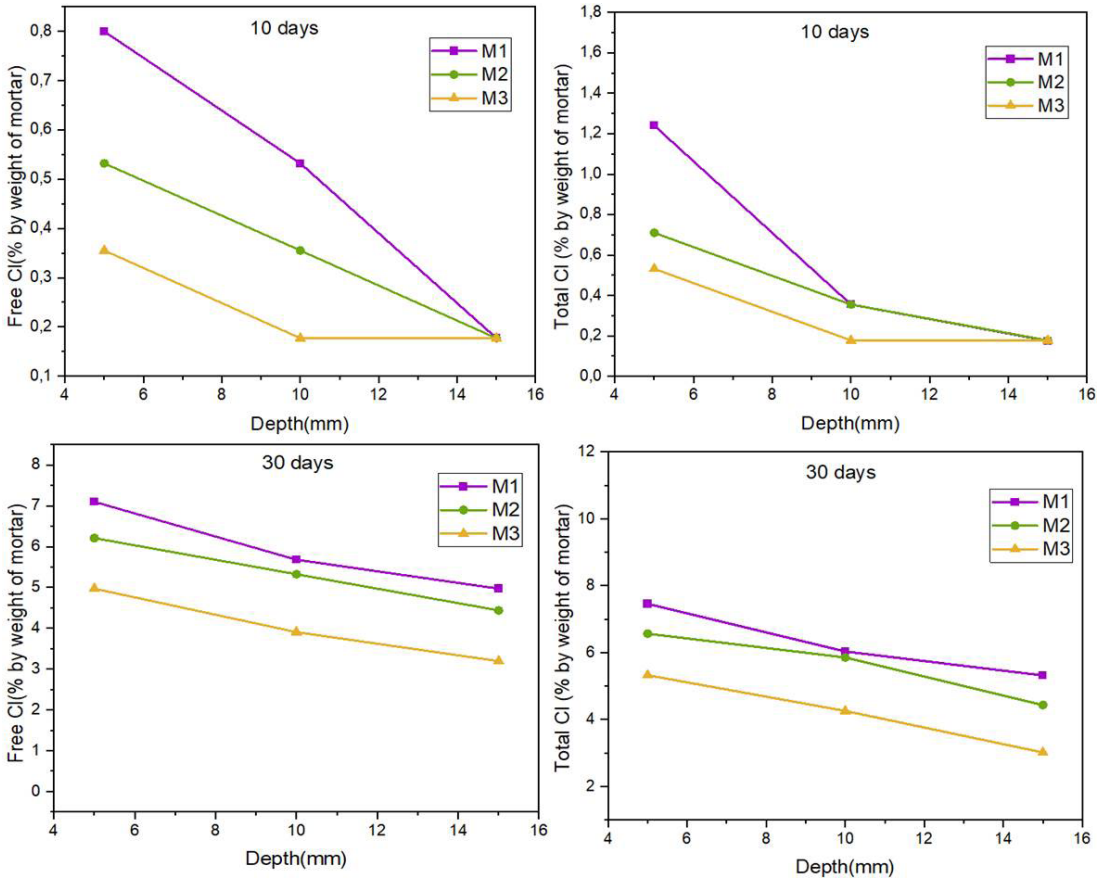

Figure 6: Free and total chloride profiles of EAFS/FA based mortars after 10 and 30 days of exposure to saline solution.

of chemical binding capacity for aluminosilicate dominated materials has been previously reported in the literature [32]. There are indications that pure slag-based alkali-activated materials are capable of binding chloride ions through surface adsorption and inter-layer ion-exchange in Mg-Al hydrotalcite like and AFm structures, respectively [29, 30]. The negligible chemical binding in the slag-dominated alkali-activated samples of the present study can be mostly attributed to the absence of hydrotalcite-like reaction products. The EAFS studied here has a lower Mg content compared to the samples studied in [29, 30] while the presence of FA in the mix can also have some hindering effects on the formation of hydrotalcite-like and AFm structures. The free chloride ions penetrated can therefore be explained by physical binding occurs when chloride ions sorb onto the C-S-H type gel surface and occurs due to electrostatic or van der Waals forces between chloride and the gel. Chloride ions can also chemically interact with C-S-H gel by several mechanisms such as chemisorption into the C-S-H layers, in C-S-H spaces, or becoming bound in the lattice or ion exchange sites of C-S-H gel [33]. The absorption of chlorides is important in M1, which has a higher FA content than that of M3 and this can be explained by the surface area of the alkali-activated binding gel increases with FA inclusion [18, 34] and therefore contributes to higher physical absorption of chloride compared to C-A-S-H gel. Ismail et al. [4] reported that Friedel salt was not detected in their study of both GGBS, and GGBS/FA activated systems and therefore suggested that majority or all the bound chlorides will be physically adsorbed to the gel. There is limited information available on the chloride binding of AA-S/FA concrete in literature. What is possible is that the available C-S-H and aluminate phases (C-(N)-A-S-H or two layered double hydroxides) in activated GGBS contribute to the physical and chemical binding reactions [29, 35]. It can be concluded then that partial replacement of FA with various amounts of EAFS can significantly improve mortars resistance to chloride penetration by reducing their free chloride content.

Conclusion

This experimental study was conducted to produce a lightweight porous alkali activated mortar based on two Moroccan local waste materials: EAFS and class F FA as a partial replacement for cement and sand and investigate their effect on chloride diffusion properties of mortar. Despite the observation of higher porosity obtained by the swelling effect, the results have shown that inclusion of slag in AAFS mortars modifies the permeability of the material, and therefore also the diffusion of aggressive agents such as chlorides. Increasing the slag content led to the refinement of pore structure and reduced the sorptivity and restricted the transportation of chloride ions in the pastes which results in a decrease in the diffusion coefficient values, highlighting the critical role of calcium in the matrix to design durable alkali-activated concretes in marine environments. The chemistry and transport mechanisms of chloride in these binders are influenced by the dominant alkali-activation reaction products, mainly C-A-S-H and N-A-S-H binding gels, which control the ionic transport

mechanisms. An insignificant chloride binding capacity was observed in the investigated alkali-activated materials in this study. As a result, it appears that only physical binding and encapsulation of chloride ions in the pore network determined the rate of diffusion and amount of chloride bound.

Acknowledgements

Authors would like to thank ASMENT cement plant and OMRANINNOV-CNRST program (CNRST-HAO-UM5R, number: 573/2021) for their support.

Conflict of Interest

None.

References

1. Mohamed OA. 2022. Effect of immersing geopolymer slag-fly ash mortar in sulfuric acid on strength development and stability of mass. *Constr Build Mater* 341: 127786. https://doi.org/10.1016/j.conbuildmat.2022.127786
2. Mohamed O. 2018. Durability and compressive strength of high cement replacement ratio self-consolidating concrete. *Buildings* 8(11): 153. https://doi.org/10.3390/buildings8110153
3. Li Z, Liu S. 2007. Influence of slag as additive on compressive strength of fly ash-based geopolymer. *J Mater Civ Eng* 19(6): 470-474. https://doi.org/10.1061/(ASCE)0899-1561(2007)19:6(470)
4. Ismail I, Bernal SA, Provis JL, San Nicolas R, Brice DG, et al. 2013. Influence of fly ash on the water and chloride permeability of alkali-activated slag mortars and concretes. *Constr Build Mater* 48: 1187-1201. https://doi.org/10.1016/j.conbuildmat.2013.07.106
5. Gao X, Yu QL, Brouwers HJH. 2015. Characterization of alkali activated slag–fly ash blends containing nano-silica. *Constr Build Mater* 98: 397-406. https://doi.org/10.1016/j.conbuildmat.2015.08.086
6. Goretta KC, Chen N, Gutierrez-Mora F, Routbort JL, Lukey GC, et al. 2004. Solid-particle erosion of a geopolymer containing fly ash and blast-furnace slag. *Wear* 256(7-8): 714-719. https://doi.org/10.1016/S0043-1648(03)00463-0
7. El-Didamony H, Amer AA, Mohammed MS, El-Hakim MA. 2019. Fabrication and properties of autoclaved aerated concrete containing agriculture and industrial solid wastes. *J Build Eng* 22: 528-538. https://doi.org/10.1016/j.jobe.2019.01.023
8. Gu G, Xu F, Ruan S, Huang X, Zhu J, et al. 2020. Influence of precast foam on the pore structure and properties of fly ash-based geopolymer foams. *Constr Build Mater* 256: 119410. https://doi.org/10.1016/j.conbuildmat.2020.119410
9. Hou L, Li J, Lu Z, Niu Y. 202. Influence of foaming agent on cement and foam concrete. *Constr Build Mater* 280: 122399. https://doi.org/10.1016/j.conbuildmat.2021.122399
10. Fu X, Lai Z, Lai X, Lu Z, Lv S. 2016. Preparation and characteristics of magnesium phosphate cement based porous materials. *Constr Build Mater* 127: 712-723. https://doi.org/10.1016/j.conbuildmat.2016.10.041
11. Novais RM, Ascensão G, Ferreira N, Seabra MP, Labrincha JA. 2018. Influence of water and aluminium powder content on the properties of waste-containing geopolymer foams. *Ceram Int* 44(6): 6242-6249. https://doi.org/10.1016/j.ceramint.2018.01.009
12. Kioupis D, Zisimopoulou A, Tsivilis S, Kakali G. 2021. Development of porous geopolymers foamed by aluminum and zinc powders. *Ceram Int* 47(18): 26280-26292. https://doi.org/10.1016/j.ceramint.2021.06.037
13. Shuai Q, Xu Z, Yao Z, Chen X, Jiang Z, et al. 2020. Fire resistance of phosphoric acid-based geopolymer foams fabricated from metakaolin and hydrogen peroxide. *Mater Lett* 263: 127228. https://doi.org/10.1016/j.matlet.2019.127228
14. Ducman V, Korat L. 2016. Characterization of geopolymer fly-ash based foams obtained with the addition of Al powder or H_2O_2 as foaming agents. *Mater Charact* 113: 207-213. https://doi.org/10.1016/j.matchar.2016.01.019
15. Kim T, Kang C, Seo K. 2021. Development and characteristics of aerated alkali-activated slag cement mixed with zinc powder. *Materials* 14(21): 6293. https://doi.org/10.3390/ma14216293
16. Li T, Huang F, Zhu J, Tang J, Liu J. 2020. Effect of foaming gas and cement type on the thermal conductivity of foamed concrete. *Constr Build Mater* 231: 117197. https://doi.org/10.1016/j.conbuildmat.2019.117197
17. Kränzlein E, Pöllmann H, Krcmar W. 2018. Metal powders as foaming agents in fly ash based geopolymer synthesis and their impact on the structure depending on the Na/Al ratio. *Cem Concr Compos* 90: 161-168. https://doi.org/10.1016/j.cemconcomp.2018.02.009
18. Phair JW. 2006. Green chemistry for sustainable cement production and use. *Green Chem* 8(9): 763-780. https://doi.org/10.1039/b603997a
19. Neville A. 1995. Chloride attack of reinforced concrete: an overview. *Mater Struct* 28: 63-70. https://doi.org/10.1007/BF02473172
20. Hu X, Shi C, Shi Z, Zhang L. 2019. Compressive strength, pore structure and chloride transport properties of alkali-activated slag/fly ash mortars. *Cem Concr Compos* 104: 103392. https://doi.org/10.1016/j.cemconcomp.2019.103392
21. Li Z, Peethamparan S. 2018. Leaching resistance of alkali-activated slag and fly ash mortars exposed to organic acid. *Green Mater* 6(3): 117-130. https://doi.org/10.1680/jgrma.18.00021
22. Baroghel-Bouny V, Chaussadent T, Croquette G, Divet L, Gawsewitch J, et al. 2002. Caractéristiques microstructurales et propriétés relatives à la durabilité des bétons (méthodes de mesure et d'essai de laboratoire). Techniques et méthodes des Laboratoires des ponts et chaussées.
23. Nguyen TQ. 2007. Physicochemical modelling of chloride ingress into cementitious materials. Ecole des Ponts ParisTech. (Doctoral Dissertation)
24. Wang Y, Tan Y, Wang Y, Liu C. 2020. Mechanical properties and chloride permeability of green concrete mixed with fly ash and coal gangue. *Constr Build Mater* 233: 117166. https://doi.org/10.1016/j.conbuildmat.2019.117166
25. Naidu TS, Sheridan CM, van Dyk LD. 2020. Basic oxygen furnace slag: review of current and potential uses. *Miner Eng* 149: 106234. https://doi.org/10.1016/j.mineng.2020.106234
26. Brandenburg K. 2001. DIAMOND Version 2.1e Crystal Impact, GbR, Bonn, Germany.
27. Parveen P, Jindal BB, Junaid MT, Saloni S. 2019. Mechanical and microstructural study of rice husk ash geopolymer paste with ultrafine slag. *Adv Concr Constr* 8(3): 217-223.
28. Babaee M, Castel A. 2018. Chloride diffusivity, chloride threshold, and corrosion initiation in reinforced alkali-activated mortars: role of calcium, alkali, and silicate content. *Cem Concr Res* 111: 56-71. https://doi.org/10.1016/j.cemconres.2018.06.009
29. Provis JL, Myers RJ, White CE, Rose V, van Deventer JS. 2012. X-ray microtomography shows pore structure and tortuosity in alkali-activated binders. *Cem Concr Res* 42(6): 855-864. https://doi.org/10.1016/j.cemconres.2012.03.004
30. Lee NK, Lee HK. 2016. Influence of the slag content on the chloride and sulfuric acid resistances of alkali-activated fly ash/slag paste. *Cem Concr Compos* 72: 168-179. https://doi.org/10.1016/j.cemconcomp.2016.06.004
31. Bondar D, Basheer M, Nanukuttan S. 2019. Suitability of alkali activated slag/fly ash (AA-GGBS/FA) concretes for chloride environments: characterisation based on mix design and compliance testing. *Constr Build Mater* 216: 612-621. https://doi.org/10.1016/j.conbuildmat.2019.05.043

32. Škvára F, Jílek T, Kopecký L. 2005. Geopolymer materials based on fly ash. *Ceram Silikáty* 49(3): 195-204.

33. Yuan Q, Shi C, de Schutter G, Audenaert K, Deng D. 2009. Chloride binding of cement-based materials subjected to external chloride environment-a review. *Constr Build Mater* 23(1): 1-13. https://doi.org/10.1016/j.conbuildmat.2008.02.004

34. Ke X, Bernal SA, Provis JL. 2017. Uptake of chloride and carbonate by Mg-Al and Ca-Al layered double hydroxides in simulated pore solutions of alkali-activated slag cement. *Cem Concr Res* 100: 1-13. https://doi.org/10.1016/j.cemconres.2017.05.015

35. Khan MSH, Kayali O, Troitzsch U. 2016. Chloride binding capacity of hydrotalcite and the competition with carbonates in ground granulated blast furnace slag concrete. *Mater Struct* 49: 4609-4619. https://doi.org/10.1617/s11527-016-0810-z